TOPOLOGICAL MATTER

Observation of the quantum spin Hall effect up to 100 kelvin in a monolayer crystal

Sanfeng Wu,[1]*† Valla Fatemi,[1]*† Quinn D. Gibson,[2] Kenji Watanabe,[3] Takashi Taniguchi,[3] Robert J. Cava,[2] Pablo Jarillo-Herrero[1]†

A variety of monolayer crystals have been proposed to be two-dimensional topological insulators exhibiting the quantum spin Hall effect (QSHE), possibly even at high temperatures. Here we report the observation of the QSHE in monolayer tungsten ditelluride (WTe_2) at temperatures up to 100 kelvin. In the short-edge limit, the monolayer exhibits the hallmark transport conductance, ~e^2/h per edge, where e is the electron charge and *h* is Planck's constant. Moreover, a magnetic field suppresses the conductance, and the observed Zeeman-type gap indicates the existence of a Kramers degenerate point and the importance of time-reversal symmetry for protection from elastic backscattering. Our results establish the QSHE at temperatures much higher than in semiconductor heterostructures and allow for exploring topological phases in atomically thin crystals.

A time-reversal (TR) invariant topological insulator (TI) in two dimensions, also known as a quantum spin Hall (QSH) insulator, can be identified by its helical edge modes (*1–4*). So far, evidence for the helical edge mode in two-dimensional (2D) TIs, particularly quantized transport, has been limited to very low temperatures (i.e., near liquid helium temperature) in HgTe and InAs/GaSb quantum wells (*5*, *6*). In the search for high-temperature TIs, substantial efforts have focused on a variety of atomically thin materials (*7–14*), which hold the promise of advancing the field of topological physics using the tools developed for 2D crystals. However, experimental observation of the quantum spin Hall effect (QSHE) in monolayer systems is challenging, often owing to structural or chemical instabilities (*9*, *15–17*). Indications of a high-temperature QSH phase in bulk-attached bismuth bilayers have been reported (*7*, *18*, *19*), but a conclusive demonstration is still lacking.

Among the proposals for atomically thin TIs are monolayer transition metal dichalcogenides (TMDs), materials that are either 2D semiconductors or semimetals depending on their structural phase (*9*). Calculations suggest that an inverted band gap can develop in 1T′ TMD monolayers, resulting in a nontrivial Z_2 topological phase (*9*, *20*). Recent experiments have shown promising results (*12–14*), including that monolayer WTe_2 exhibits a ground state with an insulating interior and conducting edges associated with a zero-bias anomaly (*12*), distinct from its multilayer counterparts (*12*, *21*). Here we observe the QSHE in WTe_2 monolayers and identify this 2D material as an atomically layered TI with conductance ~e^2/h per edge at high temperatures, where e is the electron charge and h is Planck's constant.

QSH transport through a 2D TR-invariant TI should exhibit the following characteristics: (i) helical edge modes, characterized by an edge conductance that is approximately the quantum value of e^2/h per edge (*5*); (ii) saturation to the conductance quantum in the short-edge limit (*22*); and (iii) suppression of conductance quantization upon application of a magnetic field, owing to the loss of protection by TR symmetry (*5*, *23*, *24*). Signatures of a Zeeman gap should be seen if the Kramers degeneracy (Dirac point) is located inside the bulk band gap. To date, simultaneous observation of the above criteria in existing 2D TI systems is still lacking (*5*, *6*, *22*, *23*, *25*), prompting the search for new QSH materials.

To check the above criteria in monolayer WTe_2, we fabricated devices with the structure depicted in Fig. 1A [see (*26*) and figs. S1 and S2]. The goal of the design was threefold: to ensure an atomically flat, chemically protected channel (no flake bending or exposure) by fully encapsulating the flake with hexagonal boron nitride (*15*, *21*); to minimize the effect of contact resistance; and to enable a length-dependence study on a single device. Our devices generally contain eight contact electrodes, a top graphite gate, and a series of in-channel local bottom gates with length L_c varying from 50 to 900 nm. The monolayer flakes are carefully selected to have a long strip shape, typically a few μm wide and about 10 μm long (table S1). Figure 1B shows a typical measurement of the four-probe conductance (in device 1) across all the local gates (~8 μm long) as a function of top-gate voltage, V_{tg}. A finite conductance plateau develops around V_{tg} = 0 V. This characteristic feature for monolayer WTe_2 stems from conduction along the edges (*12*). The measured value is highly sensitive to contact properties (*12*), which prevents observation of the intrinsic edge conductance. We overcome this obstacle in our devices through selective doping of the flake using a combination of global top and local bottom gates. A short transport channel with length L_c can be selectively defined by a local gate voltage V_c, whereas the rest of the flake is highly doped by V_{tg} to secure good contact to the electrodes (see fig. S3 for dI/dV characteristics, where dI ~ 1 nA is the applied ac current). Figure 1C maps out the resistance R in the same device as a function of V_{tg} and V_c (for a local gate with L_c = 100 nm). The step structure indicates a transition from a bulk-metallic state (doped) to a bulk-insulating state (undoped) within the locally gated region. We define the offset resistance, $\Delta R = R(V_c) - R(V_c = -1V)$, as the resistance change from the value in the highly doped limit (V_c = –1V, in this case). Figure 1D shows a ΔR trace (red curve) extracted from Fig. 1C (dashed white line in Fig. 1C), where V_{tg} is fixed at 3.5 V. The average value of ΔR at the plateau, which measures the step height, saturates when V_{tg} is high enough (Fig. 1D, inset, and figs. S4 to S7).

This saturated value, ΔR_s, thus measures the resistance of the undoped channel, which can only originate from the edges because the monolayer interior is insulating (*12–14*). Notably, ΔR_s is approximately equal to $h/2e^2$ for both this 100-nm channel and the 60- and 70-nm channels on device 2 (Fig. 1D). Fluctuations in the range of a few kilohm, which may originate from residual disorder or correlation effects (*12*, *27*, *28*), are visible, but decrease substantially above 4 K. Given that the sample has two edges, the observed conductance per edge is therefore ~e^2/h, pointing to helical edge modes as the source of the conductance (*5*, *6*). To confirm this scenario, one must rule out the possibility of trivial diffusive edge modes that happen to exhibit the quantized conductance value for some particular length (*22*). We thus performed a length-dependence study using a series of local gates with different L_c. Detailed analysis of measurements from representative devices and gates at ~4 K can be found in figs. S3 to S5. In Fig. 2, we summarize the data by plotting the undoped-channel resistance, ΔR_s, as a function of L_c. For long edges, the resistance generally decreases with decreasing length, which is arguably captured by a linear trend. The behavior, however, clearly deviates from the trend when L_c is reduced to 100 nm or less, where the resistance saturates to a value close to $h/2e^2$. Such behavior is present in all three devices that enter this short-length regime, independent of the width of the monolayer flake (varying from 1 to 4 μm). These observations reveal the intrinsic conductance as e^2/h per edge, as per the abovementioned criteria (i) and (ii) for the QSHE.

To check criterion (iii), regarding TR symmetry protection from elastic scattering, we performed magnetoconductance measurements. The data

[1]Department of Physics, Massachusetts Institute of Technology (MIT), Cambridge, MA 02139, USA. [2]Department of Chemistry, Princeton University, Princeton, NJ 08544, USA. [3]Advanced Materials Laboratory, National Institute for Materials Science, 1-1 Namiki, Tsukuba 305-0044, Japan.
*These authors contributed equally to this work.
†Corresponding author. Email: swu02@mit.edu (S.W.); vfatemi@mit.edu (V.F.); pjarillo@mit.edu (P.J.-H.)

Downloaded from http://science.sciencemag.org/ on February 16, 2018

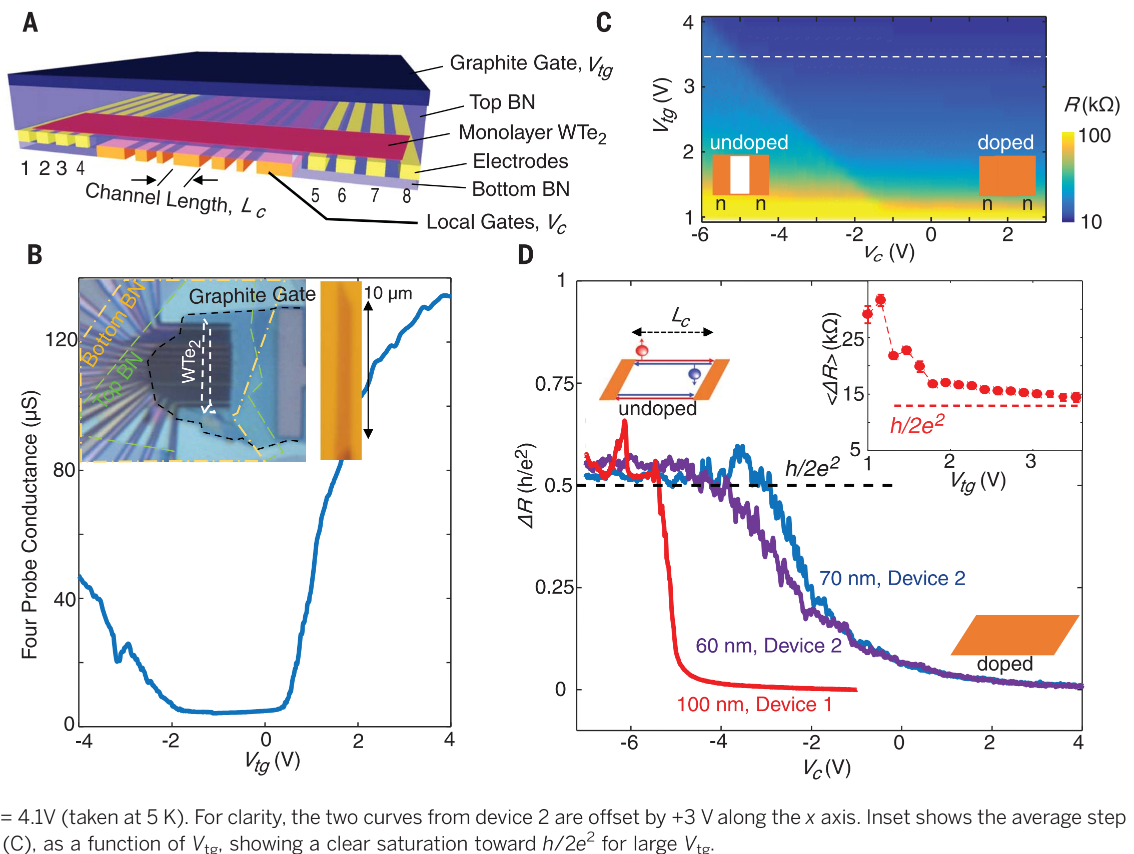

Fig. 1. Device structure and resistance near $h/2e^2$. (**A**) Schematic of the device structure. BN, boron nitride. (**B**) Four-probe conductance measurement at 4 K of device 1 as a function of V_{tg} across all the local gates, which are floating. Inset shows the optical image of device 1 (left) and the corresponding monolayer WTe_2 flake before fabrication (right). (**C**) Color map of the flake resistance tuned by V_{tg} and the 100-nm-wide local gate V_c at 4 K. Two regions are separated by a step in the resistance, which distinguishes the doped and undoped local channels, as depicted by the inset schematics. Ω, ohm. (**D**) ΔR versus V_c for the 100-nm-wide gate on device 1 at V_{tg} = 3.5 V [white dashed line in (C)] and the 60- and 70-nm-wide gates on device 2 at V_{tg} = 4.1V (taken at 5 K). For clarity, the two curves from device 2 are offset by +3 V along the *x* axis. Inset shows the average step height <ΔR>, extracted from (C), as a function of V_{tg}, showing a clear saturation toward $h/2e^2$ for large V_{tg}.

taken from the 100-nm-long channel in device 1 in the QSHE regime (i.e., gate range of the plateau) are shown in Fig. 3. We define G_s as $1/\Delta R_s$, which measures the conductance of the edges in the short channel limit. G_s is plotted as a function of V_c in Fig. 3A for a series of magnetic fields *B* applied perpendicular to the monolayer at 1.6 K. G_s decreases substantially once *B* is turned on, in contrast to the bulk state, which is hardly affected (fig. S8). For all V_c, G_s decreases rapidly for low magnetic fields (B < 2 T). After this initial stage, two types of behavior are observed, depending on V_c, as shown in Fig. 3B. When V_c is near −6.44 V, G_s decreases exponentially without saturation, up to 8 T. For other values of V_c, G_s saturates at high *B*. These behaviors are notably different from the previous observations for resistive channels (*12*).

Both types of behavior can be understood in the context of the QSHE. The 1D edge state of the QSH phase consists of two species: left and right movers associated with opposite spin polarization. The two linearly dispersing bands cross at the Kramers degeneracy point (Fig. 3B, inset I). Magnetic fields applied nonparallel to the spin polarization are expected to open an energy gap at the Kramers point owing to the Zeeman effect (*29*). For a homogeneous chemical potential close to the degeneracy point (Fig. 3B, inset II), one would expect an exponential decay of the conductance without saturation. To reveal the existence of the gap, we performed temperature-

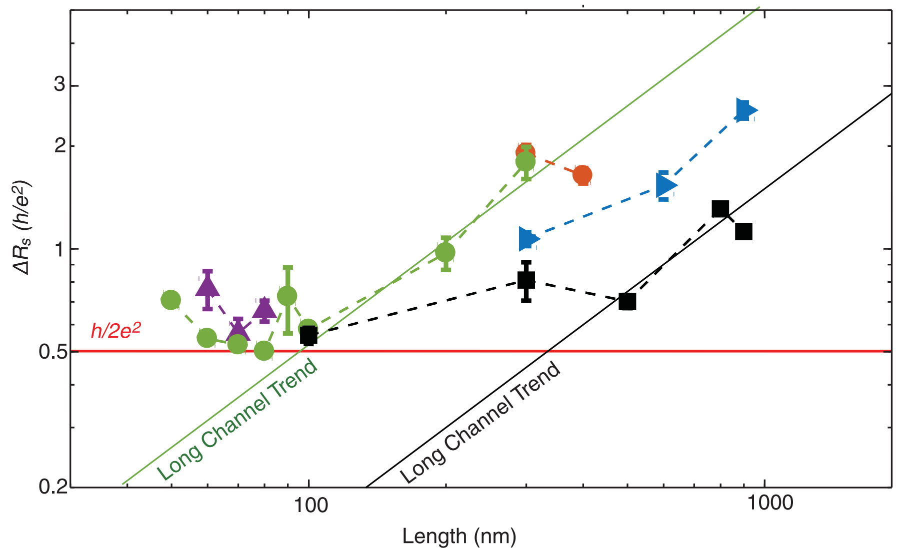

Fig. 2. Length dependence of the undoped-channel resistance. Data taken at 4 K from five different devices (table S1), each denoted by a different color and symbol. The device numbers and associated colors are: 1, black; 2, green; 3, purple; 4, red; and 5, blue. The ΔR_s values approach a minimum of $h/2e^2$ in the short-channel limit, confirming a total conductance of $2e^2/h$ for the undoped channel, i.e., a conductance of e^2/h per edge in the device, in agreement with QSHE. Detailed analysis of raw data can be found in figs. S4 to S7.

dependence measurements of the magnetoconductance at V_c = −6.44 V. The exponential decay of G_s persists up to high temperatures (measured up to 34 K, inset of Fig. 3C). Moreover, all the curves collapse onto a single universal trend when renormalized by plotting the dimensionless values $-\log(G_s/G_0)$ versus $\mu_B B/k_B T$ (Fig. 3C), where G_0 is the zero-field conductance, μ_B is the Bohr magneton, k_B is the Boltzmann constant, and *T* is the temperature. The slope of the trend

Downloaded from http://science.sciencemag.org/ on February 16, 2018

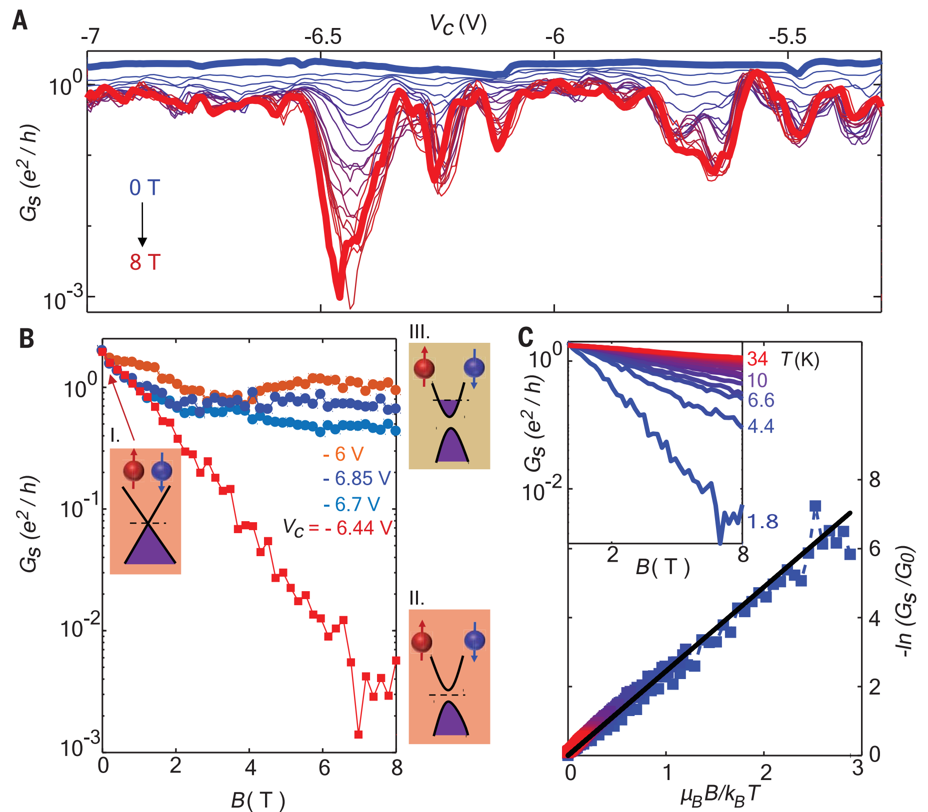

Fig. 3. Magnetoconductance and Zeeman-like gap at the Dirac point. (**A**) The evolution of the edge conductance G_s versus local gate voltage V_c under the application of a perpendicular magnetic field, B (from 0 T, thick blue curve, to 8 T, thick red curve, in 0.2-T steps) at 1.8 K, for device 1, 100-nm channel. (**B**) Traces of G_s versus B for a few selected V_c, showing two types of behavior, saturation and nonsaturation, associated with whether the Fermi energy (E_F) is in the Zeeman gap, as depicted in the band schematics inset I (linear bands at zero B, E_F at Dirac point), II (gapped bands at finite B, E_F at Dirac point), and III (gapped bands at finite B, E_F away from Dirac point). Red and blue spheres illustrate the opposite spin polarization of the edge bands, respectively. Purple areas indicate the filled bands. (**C**) Inset shows temperature dependence of G_s versus B for the nonsaturating curves (V_c = −6.44 V). All the curves in the inset collapse to a single trend in the normalized plot of $-\log(G_s/G_0)$ versus $\mu_B B/k_B T$. The black line is a linear fit. Additional temperature and magnetic field dependence is shown in figs. S9 to S11.

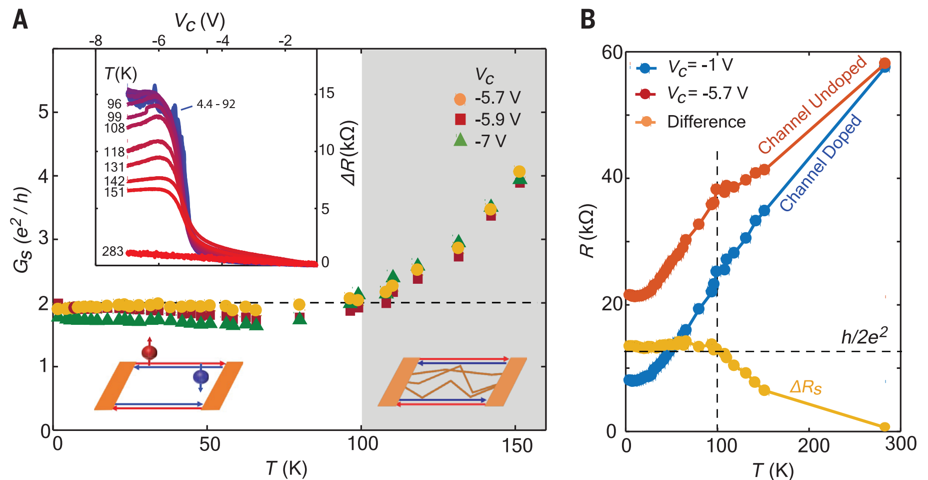

Fig. 4. Quantum spin Hall effect up to 100 K. (**A**) Temperature dependence of the edge conductance at a few representative gate voltages for the 100-nm channel in device 1. The conductance is dominated by the QSHE up to about 100 K. The right schematic depicts the onset of bulk-state contribution to the conductance. Inset shows gate dependence of ΔR at various temperatures. (**B**) Temperature dependence of the resistance of the whole flake (full length) when the Fermi energy in the local channel is in the doped (V_c = −1 V, red) and undoped (V_c = −5.7 V, blue) regimes, at V_{tg} = 3.5 V. The difference between the curves yields the temperature-dependent channel resistance ΔR_s (yellow). The vertical dashed line highlights the kink in the undoped regime at 100 K, indicating the transition to the QSHE edge-dominated regime.

yields an effective g-factor ~4.8 for the out-of-plane field in this device [i.e., the device conductance obeys $G_s = G_0 \exp(-g\mu_B B/2k_B T)$]. This observation confirms a Zeeman-type gap opening in the edge bands.

If the Fermi energy at the edge is gated away from the Kramers degeneracy point (Fig. 3B, inset III), the Zeeman gap will not be directly observed, and the magnetoconductance should be determined by the scattering mechanisms at the edge allowed by the TR symmetry breaking. For example, in our devices, the presence of local charge puddles can be natural. According to theoretical calculations, the edge conductance will be reduced to $\alpha e^2/h$, where α is a field-dependent coefficient determined by the microscopic details of the edge (*24*, *30*). Calculations show that, at high magnetic fields, an individual puddle can reduce transmission along an edge by 50% (*24*, *31*), leading to a saturated α determined by the distribution of the puddles along the edges. We find the conductance saturation is consistent with this picture (fig. S9). In addition to vertical magnetic fields, we have also found considerably reduced edge conductance when in-plane magnetic field is applied (fig. S10). We expect that both in- and out-of-plane magnetic fields will suppress the conductance: TR symmetry removes protection of the edge conduction, and the edge-mode spin-polarization axis is not necessarily normal or parallel to the layer because the monolayer lacks out-of-plane mirror symmetry. The exact spin-polarization axis may be influenced by multiple factors, such as the direction of the crystallographic edge and the existence of displacement electric fields. The irregular edge of the exfoliated monolayer makes the situation more complex. Overall, the magnetoconductance behavior is consistent with criterion (iii). Therefore, the QSHE is indeed observed in monolayer WTe_2.

Notably, the distinctive zero-field conductance value survives up to high temperatures. Figure 4A plots the temperature dependence of G_s at different V_c in the QSHE regime; G_s stays

Downloaded from http://science.sciencemag.org/ on February 16, 2018

approximately constant and close to $2e^2/h$ up to 100 K, indicating that the conductance is dominated by the QSHE up to this temperature. In terms of ΔR, the resistance plateau starts to drop at around 100 K (Fig. 4A, inset). We note that it is not obvious a priori what the temperature dependence of the QSH edge conductance should be, and some proposed mechanisms indicate weak (*32*) or even negative temperature dependence (*27*). Above 100 K, the channel conductance increases rapidly with temperature, indicating the activation of bulk-conduction channels. To reveal the transition more clearly, in Fig. 4B we plot the temperature dependence of the resistance R of the whole flake (i.e., the entire length, which consists of the locally gated region in series with the rest of the flake) when the chemical potential in the local channel is placed in the metallic regime (V_c = –1 V) and the QSH regime (V_c < –5.3 V). A clear kink at 100 K can be seen in the QSH regime. The difference between the two curves yields the channel resistance, which drops above the transition temperature.

This high-temperature QSHE is consistent with the prediction of a large inverted band gap (~100 meV) in monolayer WTe_2 (*20*) as well as recent experiments that observe a ~45-meV bulk band gap in spectroscopy (*13*, *14*) and a similar onset temperature for bulk conduction (*12*). We suspect the 100 K transition temperature may not be an intrinsic limit. Improvements in device quality may enable observation of the QSHE at even higher temperatures and for longer edges.

Our observations have confirmed the nontrivial TR invariant topological phase in monolayer WTe_2 and demonstrated the QSHE at high temperatures in an isolated 2D monolayer device. The exploration of 2D topological physics and device performance above liquid nitrogen temperatures has therefore become possible. Distinct from quantum well systems, the exposed nature of isolated monolayers may allow for engineering topological phases in unprecedented ways. In particular, WTe_2 can be readily combined with other 2D materials to form van der Waals heterostructures, a promising platform for studying the proximity effect between a QSH system and superconductors or magnets (*3*, *4*) at the atomic scale.

REFERENCES AND NOTES

1. C. L. Kane, E. J. Mele, *Phys. Rev. Lett.* **95**, 226801 (2005).
2. B. A. Bernevig, S.-C. Zhang, *Phys. Rev. Lett.* **96**, 106802 (2006).
3. M. Z. Hasan, C. L. Kane, *Rev. Mod. Phys.* **82**, 3045–3067 (2010).
4. X.-L. Qi, S.-C. Zhang, *Rev. Mod. Phys.* **83**, 1057–1110 (2011).
5. M. König *et al.*, *Science* **318**, 766–770 (2007).
6. I. Knez, R.-R. Du, G. Sullivan, *Phys. Rev. Lett.* **107**, 136603 (2011).
7. S. Murakami, *Phys. Rev. Lett.* **97**, 236805 (2006).
8. Y. Xu *et al.*, *Phys. Rev. Lett.* **111**, 136804 (2013).
9. X. Qian, J. Liu, L. Fu, J. Li, *Science* **346**, 1344–1347 (2014).
10. J.-J. Zhou, W. Feng, C.-C. Liu, S. Guan, Y. Yao, *Nano Lett.* **14**, 4767–4771 (2014).
11. S. S. Li *et al.*, *Sci. Rep.* **6**, 23242 (2016).
12. Z. Fei *et al.*, *Nat. Phys.* **13**, 677–682 (2017).
13. S. Tang *et al.*, *Nat. Phys.* **13**, 683–687 (2017).
14. Z.-Y. Jia *et al.*, *Phys. Rev. B* **96**, 041108 (2017).
15. Y. Cao *et al.*, *Nano Lett.* **15**, 4914–4921 (2015).
16. L. Wang *et al.*, *Nat. Commun.* **6**, 8892 (2015).
17. F. Ye *et al.*, *Small* **12**, 5802–5808 (2016).
18. C. Sabater *et al.*, *Phys. Rev. Lett.* **110**, 176802 (2013).
19. I. K. Drozdov *et al.*, *Nat. Phys.* **10**, 664–669 (2014).
20. F. Zheng *et al.*, *Adv. Mater.* **28**, 4845–4851 (2016).
21. V. Fatemi *et al.*, *Phys. Rev. B* **95**, 041410 (2017).
22. F. Nichele *et al.*, *New J. Phys.* **18**, 083005 (2016).
23. E. Y. Ma *et al.*, *Nat. Commun.* **6**, 7252 (2015).
24. S. Essert, K. Richter, *2D Mater* **2**, 024005 (2015).
25. L. Du, I. Knez, G. Sullivan, R.-R. Du, *Phys. Rev. Lett.* **114**, 096802 (2015).
26. See supplementary materials.
27. J. Maciejko *et al.*, *Phys. Rev. Lett.* **102**, 256803 (2009).
28. T. Li *et al.*, *Phys. Rev. Lett.* **115**, 136804 (2015).
29. M. König *et al.*, *J. Phys. Soc. Jpn.* **77**, 031007 (2008).
30. J. Maciejko, X.-L. Qi, S.-C. Zhang, *Phys. Rev. B* **82**, 155310 (2010).
31. A. Roth *et al.*, *Science* **325**, 294–297 (2009).
32. J. I. Väyrynen, M. Goldstein, Y. Gefen, L. I. Glazman, *Phys. Rev. B* **90**, 115309 (2014).

ACKNOWLEDGMENTS

We thank L. Fu and X. Qian for helpful discussions. This work was partly supported through Air Force Research Laboratory grant no. FA9550-16-1-0382 as well as the Gordon and Betty Moore Foundation's Emergent Phenomena in Quantum Systems (EPiQS) Initiative through grant no. GBMF4541 to P.J.-H. Device nanofabrication was partly supported by the Center for Excitonics, an Energy Frontier Research Center funded by the U.S. Department of Energy, Basic Energy Sciences Office, under award no. DE-SC0001088. This work made use of the Materials Research Science and Engineering Center's shared experimental facilities supported by the NSF under award no. DMR-0819762. Sample fabrication was performed in part at the Harvard Center for Nanoscale Science supported by the NSF under grant no. ECS-0335765. S.W. acknowledges the support of the MIT Pappalardo Fellowship in Physics. The WTe_2 crystal growth performed at Princeton University was supported by the NSF Materials Research Science and Engineering Center (MRSEC) grant DMR-1420541. Growth of hexagonal boron nitride crystals was supported by the Elemental Strategy Initiative conducted by the Ministry of Education, Culture, Sports, Science and Technology (MEXT), Japan; and the Japan Society for the Promotion of Science (JSPS) Grants-in-Aid for Scientific Research (KAKENHI) through grant nos. JP15K21722 and JP25106006. The data presented in this paper are available from the corresponding authors upon reasonable request.

SUPPLEMENTARY MATERIALS

www.sciencemag.org/content/359/6371/76/suppl/DC1
Materials and Methods
Supplementary Text
Figs. S1 to S11
Table S1
References (*33*, *34*)

7 May 2017; accepted 17 November 2017
10.1126/science.aan6003

Downloaded from http://science.sciencemag.org/ on February 16, 2018

Science

Observation of the quantum spin Hall effect up to 100 kelvin in a monolayer crystal

Sanfeng Wu, Valla Fatemi, Quinn D. Gibson, Kenji Watanabe, Takashi Taniguchi, Robert J. Cava and Pablo Jarillo-Herrero

Science **359** (6371), 76-79.
DOI: 10.1126/science.aan6003

Heating up the quantum spin Hall effect

Taking practical advantage of the topologically protected conducting edge states of topological insulators (TIs) has proven difficult. Semiconductor systems that have been identified as two-dimensional TIs must be cooled down to near liquid helium temperatures to bring out their topological character. Wu *et al.* fabricated a heterostructure consisting of a monolayer of WTe_2 placed between two layers of hexagonal boron nitride and found that its topological properties persisted up to a relatively high temperature of 100 K. Engineering this so-called quantum spin Hall effect in a van der Waals heterostructure makes it possible to apply many established experimental tools and functionalities.

Science, this issue p. 76

ARTICLE TOOLS http://science.sciencemag.org/content/359/6371/76

SUPPLEMENTARY MATERIALS http://science.sciencemag.org/content/suppl/2018/01/03/359.6371.76.DC1

REFERENCES This article cites 33 articles, 3 of which you can access for free
http://science.sciencemag.org/content/359/6371/76#BIBL

PERMISSIONS http://www.sciencemag.org/help/reprints-and-permissions

Use of this article is subject to the Terms of Service

Science (print ISSN 0036-8075; online ISSN 1095-9203) is published by the American Association for the Advancement of Science, 1200 New York Avenue NW, Washington, DC 20005. 2017 © The Authors, some rights reserved; exclusive licensee American Association for the Advancement of Science. No claim to original U.S. Government Works. The title *Science* is a registered trademark of AAAS.

Downloaded from http://science.sciencemag.org/ on February 16, 2018